Research Article

Nano Research
2023, 16(2): 2020–2025

ISSN 1998-0124 CN 11-5974/O4
https://doi.org/10.1007/s12274-022-4860-y

Fe-porphyrin: A redox-related biosensor of hydrogen molecule

Zhaokui Jin[1,2], Penghe Zhao[2], Wanjun Gong[2], Wenjiang Ding[1], and Qianjun He[1,2] (✉)

[1] *Center of Hydrogen Science, School of Materials Science and Engineering, Shanghai Jiao Tong University, 800 Dongchuan Road, Shanghai 200240, China*

[2] *School of Biomedical Engineering, Health Science Center, Shenzhen University, 1066 Xueyuan Road, Shenzhen 518060, China*

Received: 15 July 2022 / **Revised:** 29 July 2022 / **Accepted:** 1 August 2022

ABSTRACT

Hydrogen molecule (H_2) exhibits broad-spectrum but microenvironment-dependent biomedical effects in varied oxidation stress-related diseases, but its molecular mechanism is unclear and its targeting molecule is unknown so far. Herein, we originally reveal that Fe-porphyrin is a H_2-targeted molecule. We have demonstrated that the oxidized Fe-porphyrin in both free and protein-confining states can self-catalyze the hydrogenation/reduction by reacting with H_2 to catalytically scavenge ·OH, and can also catalytically hydrogenate to reduce CO_2 into CO in the hypoxic microenvironment of *in vitro* simulation and *in vivo* tumor, confirming that Fe-porphyrin is a redox-related biosensor of H_2 and H_2 is an upstream signaling molecule of CO. These discoveries are favorable for deep understanding and exploration of profound biomedical effects of H_2, and helpful for development of innovative drugs and hydrogen energy/agricultural materials.

KEYWORDS

hydrogen molecule, molecular mechanism, molecular target, hydrogen medicine, porphyrin, catalysis, carbon monoxide

1 Introduction

Hydrogen molecule (H_2) has proven to have a broad-spectrum biomedical effect in a variety of oxidation stress-related diseases [1–6], but its molecular targeting point is not clear. In the current popular opinion, H_2 can selectively scavenge highly toxic reactive oxygen species (ROS) such as ·OH [2], but in principle, the reaction rate of H_2 with ·OH is considerably low owing to high activation energy and low solubility of H_2 in water (1.6 ppm) [7], implying little probability of direct reaction. Therefore, we here speculate that there could be an enzyme/sensor for catalyzing the H_2-related reaction in the body.

Besides the anti-inflammatory effect in general inflammation-related diseases, we have recently discovered that H_2 also exhibited a pro-inflammatory effect and induced oxidation stress in the tumor microenvironment (TME) [8–10]. It hints the biological behaviors of H_2 are possibly dependent on the specific microenvironment. Moreover, these two effects of H_2 in inflammation and cancer are highly similar to that of CO molecules. Therefore, we here hypothesize that H_2 possibly is an upstream signaling molecule of CO for playing its biomedical effects.

The catalytic center of hydrogenase in anaerobes is located on the S/Fe/Ni-coordinated Fe [11], and the signal transduction of CO is mainly initiated from the coordination between CO and ferrous porphyrin [12, 13]. Therefore, we here envisage that the N-coordinated Fe in ferrous porphyrin could possibly sense and decompose H_2 like hydrogenase, and then catalytically hydrogenate ROS and CO_2 to scavenge ROS and generate CO in ROS-rich and hypoxic microenvironments, respectively. Fortunately, we have verified the hypotheses with experimental evidences in this work.

2 Results and discussion

2.1 Catalytic hydrogenation activity of Fe-porphyrin

Firstly, the hydrogenation activity of Fe-porphyrin as a hydrogen biosensor is confirmed. Visually, both the bubbling of hydrogen gas (Fig. S1 in the Electronic Supplementary Material) and the addition of hydrogen-rich water (HRW, Fig. 1(b)) into the aqueous triethylamine (Et_3N) solution of hematin (Ht) cause the quick decrease of the absorption bands at 386 and 605 nm and the increase of the absorption band at 650 nm, implying the hydrogenation of Ht. Furthermore, the reaction product between Ht and H_2 (Fig. 1(a)) is confirmed to be the hydrided Fe-porphyrin (HmH), as demonstrated by ^{1}H NMR (Fig. 1(c)) and FTIR (Fig.1(d)) results. ^{1}H NMR data indicate that a single hydrogen atom (4.57 ppm) is coordinated on the Fe center of HmH (Fig. 1(c)), and FTIR data also suggest the formation of the Fe–H bond as well as the enhancement of the N–H bond (Fig. 1(d)), which is possibly due to the hydrogen bonding of Fe–H···N. The reducibility of the hydrogen coordinated with Fe in HmH is especially high, as indicated by that Ht can catalytically hydrogenate methylene blue (MB) in a rapid way (Fig. 1(e)).

In addition to the free state, Fe-porphyrin is mainly confined in the structure of many proteins such as hemoglobin (Hb) and cytochromes (Cyt) in the body, and is largely concentrated at cellular mitochondria and in red blood cells (RBC), which can be the main workplaces of H_2. Therefore, we further checked the catalytic hydrogenation activity of Fe-porphyrin in the levels of protein and cell. The oxidized Hb (HbO_2) is similar to Ht for quick reaction with H_2, and can catalytically hydrogenate O_2

Address correspondence to nanoflower@126.com

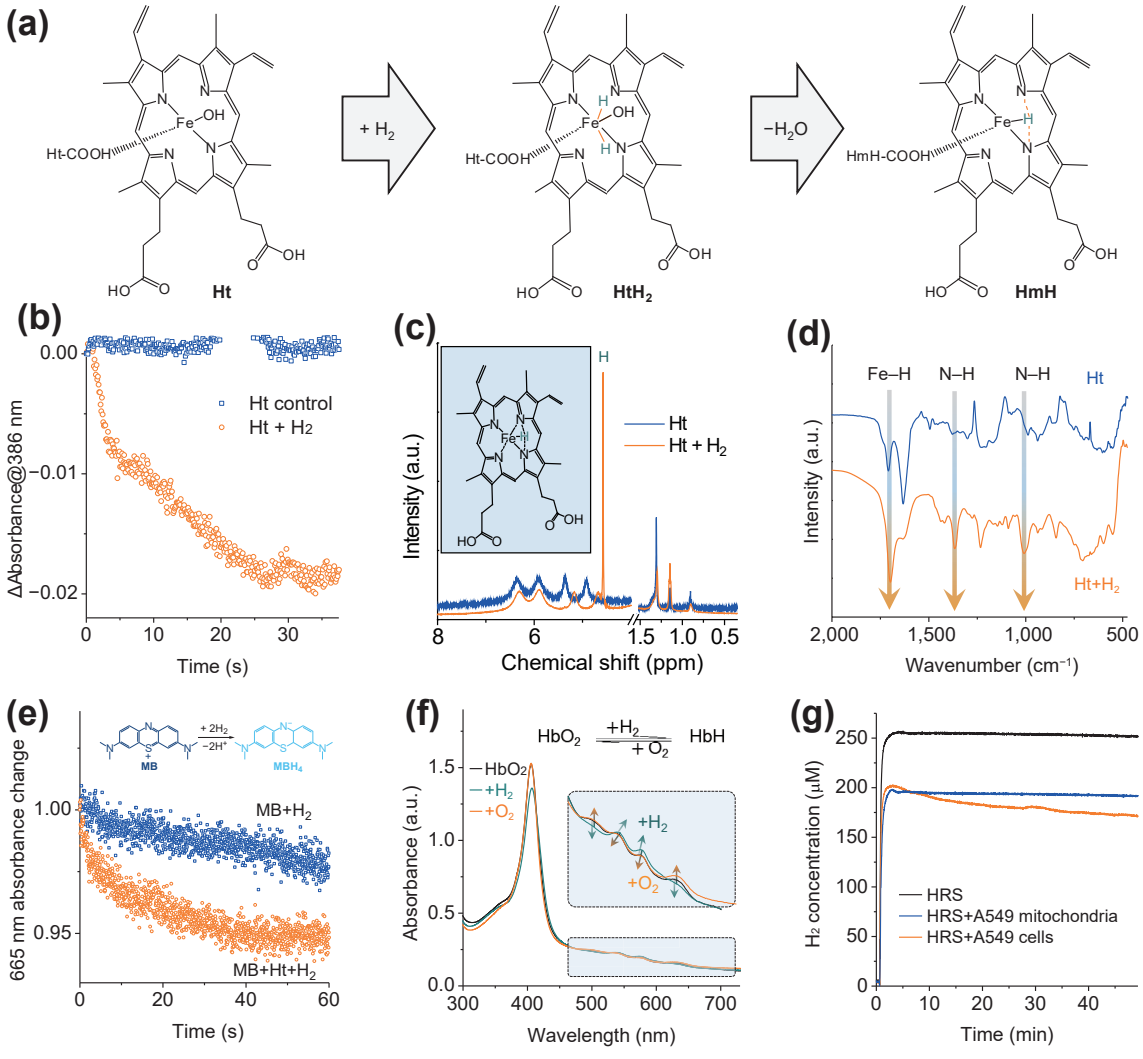

Figure 1 The catalytic hydrogenation behavior of Fe-porphyrin. (a) The proposed hydrogenation reaction of hematin (Ht), (b) the real-time monitoring of the absorbance change at 386 nm during the reaction between Ht and hydrogen-rich water (HRW), (c) ^{1}H-NMR and (d) FTIR spectra of Ht before and after reaction with H_2, (e) the methylene blue (MB) indication for the reducibility of the Ht hydrogenation product, (f) the UV absorption spectra of oxidized hemoglobin (HbO_2) before and after hydrogenation and then oxygenation, and (g) the real-time monitoring of H_2 concentration in hydrogen-rich saline (HRS) during incubation with A549 cells or their mitochondria using the hydrogen microelectrode.

slowly (Fig. 1(f)). Furthermore, A549 cells (a lung cancer cell line) can quickly consume H_2 in hydrogen-rich saline (HRS) because of containing a large amount of Fe-porphyrin proteins such as Hb and CytC (Fig. 1(g)). Moreover, extracted mitochondria from the equal amount of A549 cells can quickly consume the almost equal amount of H_2 (0.1875 pmol/cell), indicating that the mitochondrion is an intracellular main workplace of H_2 where Fe-porphyrin is able to catalytically hydrogenate/scavenge ROS and to donate electrons for offsetting the electronic leakage in the electron-transport chain. This can well explain the previous popular phenomenon that H_2 plays a role as a mitochondrial remediator under oxidation stress [14, 15].

2.2 ROS-scavenging behavior of Fe-porphyrin-catalytic hydrogenation

There are a variety of oxidative species, especially low concentration of ROS (nM level) in the mitochondria and high concentration of O_2 in the blood (about 7 mM). The catalytic hydrogenation activity and rate of Fe-porphyrin reacting with oxidative species will determine the order and degree of the competitive reactions and the biomedical effects of H_2 in the body. Therefore, we experimentally detected the kinetics of several typical ROS reacting with H_2 in the presence and absence of Hb as a typical Fe-porphyrin catalyst. From Fig. 2, Hb can catalyze the hydrogenation of ·OH (Figs. 2(a) and 2(b)) more significantly than that of $ONOO^-$ (Figs. 2(c) and 2(d)) and H_2O_2 (Figs. 2(e) and 2(f)), meaning that H_2 will preferentially scavenge ·OH prior to other ROS under the catalysis of Hb, possibly because of higher oxidability and smaller dimension of ·OH. Small dimension is thought to be favorable for ROS and H_2 to enter into the porous channel of Hb protein to react with Fe-porphyrin there. This well explains the previous phenomenon of H_2 selectively scavenging highly cytotoxic ·OH rather than other ROS [2]. In addition, it is worth noting that the concentration of O_2 in the body, especially in the blood, is distinctly higher than that of ROS, implying that there is a certain probability of O_2 hydrogenation in an oxygen-rich microenvironment under the catalysis of Fe-porphyrin (Fig. 1(f)). This drops us a hint that the remote diffusion-mediated delivery of H_2 through the blood circulation might be relatively lowly efficient, and the mitochondria-targeted delivery and local release of H_2 could possibly bring benefit for hydrogen therapy of diseases.

2.3 CO-generating behavior of Fe-porphyrin-catalytic CO_2 hydrogenation in the hypoxic microenvironment

Since the concentration of CO_2 in the body, especially in the mitochondria, is considerably high, we checked whether CO_2 can be reduced by H_2 into CO through Fe-porphyrin-catalytic

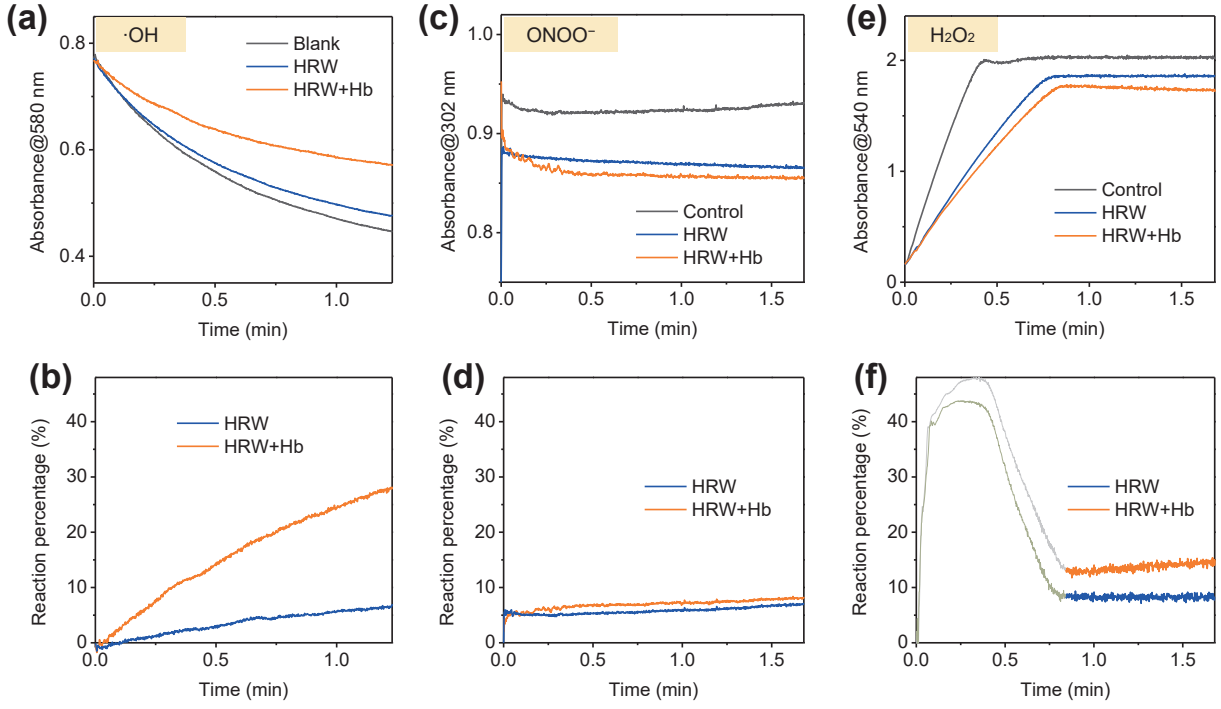

Figure 2 The catalytic ROS-scavenging behavior of H_2. ((a), (c), and (e)) The dynamic curves of ROS reaction with H_2 in the presence and absence of Hb, where ·OH (a), $ONOO^-$ (c), and H_2O_2 (e) were detected by their colorimetric probes (methyl violet for ·OH, and 4-aminoantipyrine/peroxidase for H_2O_2) or intrinsic absorption ($ONOO^-$, at 302 nm). ((b), (d), and (f)) The calculated percentages of ·OH (b), $ONOO^-$ (d), and H_2O_2 (f) reaction with H_2 according to the corresponding dynamic curves. In (f), the curves (gray) before 0.84 min mainly involved the detection reaction, which did not reflect the early hydrogenation of H_2O_2.

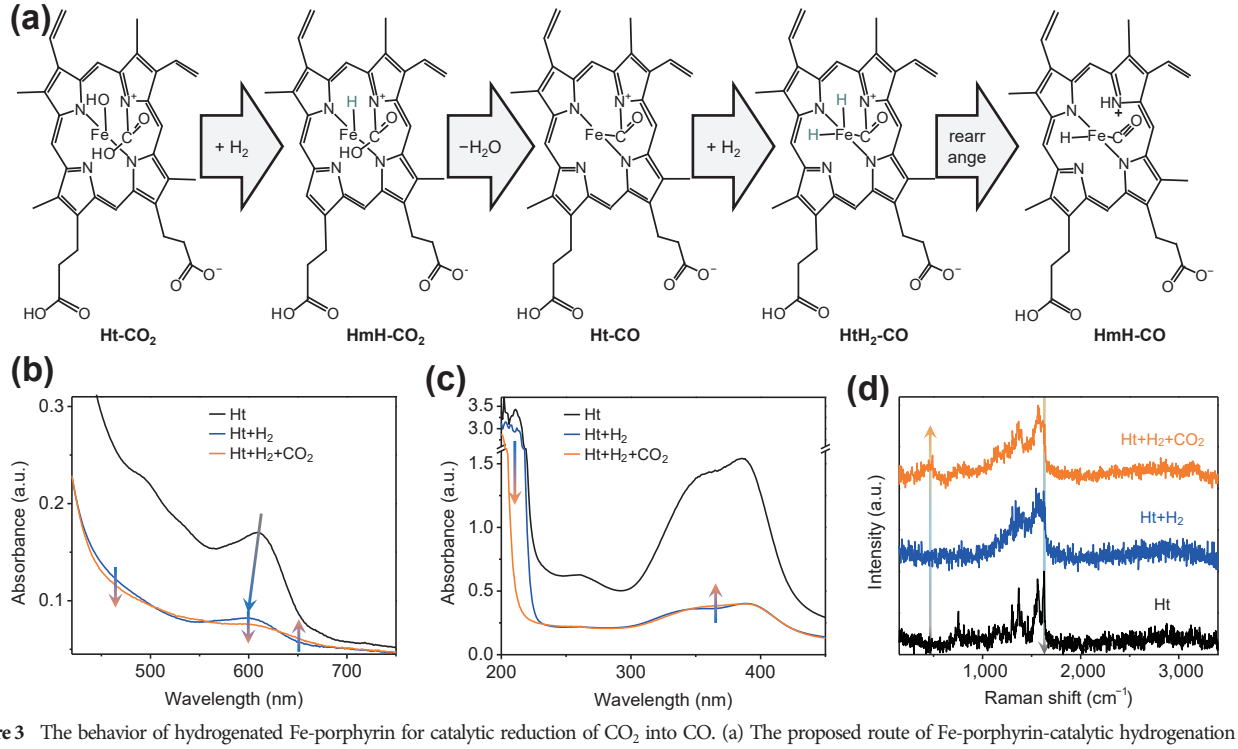

Figure 3 The behavior of hydrogenated Fe-porphyrin for catalytic reduction of CO_2 into CO. (a) The proposed route of Fe-porphyrin-catalytic hydrogenation and CO_2 reduction, and the UV ((b), (c)) and Raman (d) spectra of the products after the hydrogenation and carbonylation of Ht.

hydrogenation (Fig. 3(a)). Excitingly, we here find that Fe-porphyrin in the free (Ht) and protein-confined (Hb) states can indeed catalyze the reduction of CO_2 into CO at the saturated aqueous solution of H_2 (800 μM) and CO_2 (33 mM), as suggested by the characteristic adsorption (Figs. 3(b) and 3(c)) and Raman (Fig. 3(d)) bands of carbonyl products. After the Et_3N solution of Ht was blown with H_2 and CO_2 gases, the product was precipitated by addition of HCl and then freshly collected for FTIR and Raman measurement. From UV spectra in Figs. 3(b) and 3(c), the decrease of absorption bands at about 600 nm and 460 nm and the increase of absorption bands at about 650 nm and 365 nm reflect the typical carbonylation of Fe-porphyrin in the hydrogenated/reduced Ht (HmH). The similar hydrogenation and carbonylation transformations are also clearly visible for Hb after H_2 and CO_2 bubbling (Fig. S2 in the ESM). From Raman spectra in Fig. 3(d), the appearance of Fe−CO peak at 460 cm^{-1} and the attenuation of *v10* band at 1,620 cm^{-1} indicate the local coordination of generated CO with reduced Fe-porphyrin, which will directly mediate the downstream CO signaling pathways.

Furthermore, we checked the possibility of catalytic CO

generation in the tumor where there is a typical hypoxic microenvironment in favor of catalytic hydrogenation and reduction. Before and after intratumoral injection of saturated HRS, photoacoustic (PA) imaging was executed on the tumors of mice, and the PA signal at 840 nm was collected to reflect local CO generation because the molar extinction coefficient of carbonylated Hb (COHb) is remarkably lower than that of other Hb proteins including oxidized and reduced ones. The sharp attenuation of PA signal at 840 nm (blue in Figs. 4(a) and 4(b), and Fig. 4(c)) once intratumoral injection of HRS suggests the quick increase of COHb content in tumor. Moreover, the decrease in Hb content (Fig. 4(d)) also means the transformation of Hb into COHb. The local generation of COHb in tumor after hydrogen administration confirms that H_2 is an upstream signaling molecule of CO. Therefore, the delivery of H_2 can play a role of CO therapy in the hypoxic microenvironment of diseases such as tumor, myocardial infarction and wound, which well explains why many biological effects of H_2 including anti-inflammation and anti-cancer seem similar with that of CO. In addition, the gradual recovery of PA signal 20 min after local HRS injection (Fig. 4) might be due to the tumor metabolism of COHb. It implies that targeted/local and sustained H_2 supply could bring great benefit for hypoxia-related diseases through CO pathway.

3 Conclusions

In summary, we have originally discovered that Fe-porphyrin is a redox-related biocatalyst/biosensor of hydrogen molecule. In the ROS-rich microenvironment such as mitochondria, Fe-porphyrin can catalyze the hydrogenation and scavenging of ROS, especially ·OH. In the hypoxic microenvironment, Fe-porphyrin can catalyze the hydrogenation and reduction of CO_2 into CO which is locally coordinated with Fe-porphyrin to mediate the downstream CO signaling pathways. These important findings will greatly help with the deep understanding of biomedical effects of hydrogen molecule, and provide inspiration for development of the rational and customized H_2 delivery systems for various major diseases.

Based on present findings, some extended new issues are proposed to be addressed in the future in favor of deeper understanding and better applications of hydrogen molecule, including that (1) whether other transition metals-caged porphyrin molecules/proteins/enzymes can also play the Fe-porphyrin-similar catalyst/sensor role; (2) whether NO can also be generated through catalytic reduction of oxynitrides by the similar catalytic route to play a downstream signaling role; (3) whether the hydrided Fe-porphyrin in blood red cells is subject to oxygenation to affect the remote delivery of active hydrogen to a certain extent; (4) whether the excessive Fe-porphyrin-catalytic hydrogenation will cause oxidation stress to generate some unexpected positive or negative effects; (5) whether H_2 can block the Fenton-like reaction based on Fe/Mn/Zn-porphyrin to intercept the progression of related diseases such as neurodegenerative diseases, chronic liver diseases and amyotrophic lateral sclerosis; (6) whether the Mg-porphyrin in chlorophyll can play the Fe-porphyrin-similar catalyst/sensor role; (7) whether transition metals-coordinated porphyrin and the molecules with the similar coordination structure can be used in hydrogen energy and agriculture for hydrogen storage, transformation, delivery and utilization, etc.

4 Experimental section

4.1 Measurement of Ht hydrogenation

Ht (Aladdin, H104216) was completely dissolved into a 1% aqueous solution of Et_3N (Sigma-Aldrich, T0886) in a quartz cuvette (Ht concentration of 16 μM), and then pure hydrogen gas was bubbled into the solution. UV spectra of the solution before and after hydrogen gas bubbling were collected (Agilent Technologies, Cary 60). On the other hand, the reaction dynamics was monitored by UV absorption at 386 nm once HRW (1 mL) was added into the oxygen-removed solution of Ht (36.5 μM, 2 mL).

4.2 Identification of the hydrided Ht

Ht (16 μM) was completely dissolved into an acetone solution of HCl, and then pure hydrogen gas was bubbled into the solution. After 2.5 h, a drop of the solution was dropped onto the attenuated total reflection platform followed by hydrogen gas blowing drying and FTIR measurement (PerkinElmer, Spectrum

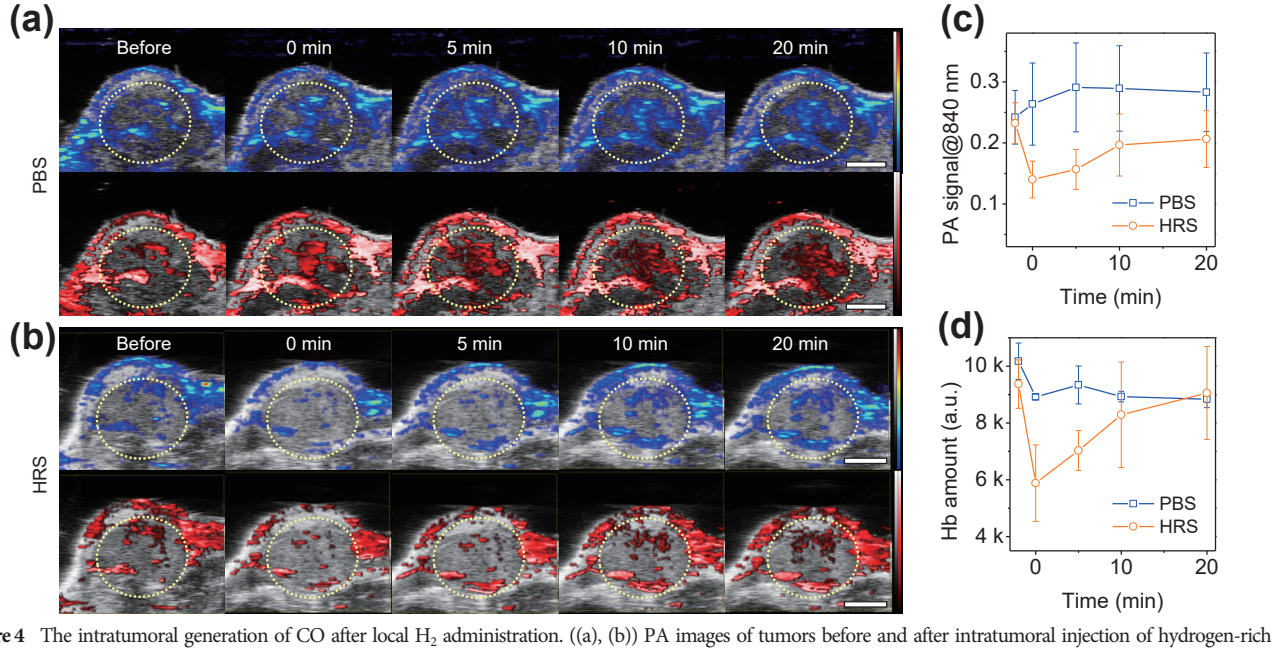

Figure 4 The intratumoral generation of CO after local H_2 administration. ((a), (b)) PA images of tumors before and after intratumoral injection of hydrogen-rich saline (HRS) for different time durations (0, 5, 10, and 20 min), and the corresponding quantification of PA intensity (c) and Hb amount (d) in the yellow dashed circles ((a), (b)) which excluded the disturbance of surface skin. The scale bars in (a) and (b) correspond to 2 mm.

Two). For ^{1}H-NMR measurement, Ht (2 mg) was completely dissolved into a mixture solution of deuterated acetone (1.5 mL, Aladdin, A100963) and deuterated HCl (20 μL, Aladdin, D304594), and then pure hydrogen gas was bubbled into the solution for 30 min, followed by NMR measurement (AVANCE NEO 400 MHz) under the protection of hydrogen gas.

4.3 Reducibility measurement of the hydrided Ht

MB (Sigma-Aldrich, 1159430025) was used as a colorimetric probe of catalytic hydrogenation. The aqueous solution of MB (2 mM, 50 μL) and the Et_3N (1%) solution of Ht (2 mM, 20 μL) in turn was added into the saturated HRW (1.93 mL) followed by dynamic monitoring at 665 nm on the UV spectrometer. As for control, Ht was not used but the concentrations of other chemicals kept the same.

4.4 Catalytic hydrogenation measurement of Hb with oxygen gas

Pure hydrogen gas was gently bubbled into the aqueous solution of Hb (50 μM, Macklin, H828504) for 10 min, and then pure oxygen gas was gently bubbled into the solution for 40 min. Before and after gas bubbling, UV spectra of the solution were collected.

4.5 Catalytic hydrogenation measurement in the cell level

A549 cells (1.08×10^6) were dispersed into the saturated HRS (1.5 mL) and then put into a microrespiration bottle for real-time monitoring of H_2 concentration with a hydrogen microelectrode (UNISENSE, MR2-St-Co). Moreover, all mitochondria in 1.08×10^6 A549 cells were extracted with a mitochondria isolation kit (Solarbio, SM0020), and then immediately dispersed into the saturated HRS (1.5 mL) in the microrespiration bottle for real-time monitoring of H_2 concentration with the hydrogen microelectrode.

4.6 Measurement of reaction dynamics of catalytic scavenging of ROS

As to ·OH scavenging, ·OH was generated by the Fenton reaction and detected by its colorimetric probe methyl violet. HRW (1.4 mL), aqueous solution of methyl violet (0.5 mM, 0.2 mL), $FeSO_4$ (4 mM, 0.1 mL), Hb (3.2 mg/mL, 0.1 mL) and H_2O_2 (2 mM, 0.2 mL) were added into the quartz cuvette in turn, and the absorbance at 580 nm was monitored in real time immediately.

The concentration of $ONOO^-$ was determined by its intrinsic absorption band at 302 nm. The aqueous solution of $ONOO^-$ was freshly prepared for immediate use by adding the aqueous solution of NaOH (1.5 M) into the equal volume of aqueous mixture solution of H_2O_2 (0.7 M), HCl (0.6 M) and $NaNO_2$ (0.6 M). HRW (1.7 mL), Hb (3.2 mg/mL, 0.1 mL) and $ONOO^-$ (0.6 M, 0.2 mL) were added into the quartz cuvette in turn, and the absorbance at 302 nm was monitored in real time immediately.

The concentration of H_2O_2 was detected by its colorimetric probe (4-aminoantipyrine/peroxidase, Kyoritsu WAK-H_2O_2). A piece of the detection agent and Hb (3.2 mg/mL, 100 μL) were dissolved into HRW (1.8 mL), and then H_2O_2 (2 mM, 100 μL) was added followed by immediate dynamic monitoring of the absorbance at 540 nm.

4.7 Measurement of catalytic hydrogenation/reduction of CO_2

The Et_3N (1%) solution of Ht (10 mM, 6 mL) was bubbled with pure hydrogen gas for 40 min to form a hypoxic environment and then with pure CO_2 gas for another 30 min. Before and after H_2/CO_2 bubbling, UV spectra of the solution were collected. The aqueous solution of HCl (36.5 mM, 10 μL) was quickly added into 0.5 mL above solution, and then the precipitate was collected by centrifugation and washed with ionized water followed by Raman measurement (Thermo Fisher, DXR3xi). As to Hb, the aqueous solution of Hb (60 μM) was lightly bubbled with pure hydrogen gas for 30 min and subsequently with pure CO_2 gas for another 30 min. Before and after H_2/CO_2 bubbling, UV spectra of the solution were collected.

4.8 *In vivo* PA imaging of tumor for measurement of COHb generation

A tumor-bearing mice model was built by injecting 5×10^6 4T1 cells into the hind limb of each female BALB/c mouse (5 weeks old) which was purchased from the Guangdong Medicinal Laboratory Animal Center (Guangzhou, China). After tumors reached about 80 mm^3, 80 μL PBS or saturated HRS was injected into tumor (n=3 for independent experiments). Before and after injection, PA signals and blood oxygen saturation at 840 nm were collected. Then, the relative Hb amount was calculated according to the reported method [16, 17]. All animal experiments were carried out in strict accordance with the regulation of the Animal Ethical and Welfare Committee of Shenzhen University.

Acknowledgements

We greatly appreciate financial support from the National Natural Science Foundation of China (Nos. 51872188 and 82172078), Shenzhen Science and Technology Program (No. RCJC20210706092010008), Special Funds for the Development of Strategic Emerging Industries in Shenzhen (No. 20180309154519685), and Center of Hydrogen Science, Shanghai Jiao Tong University, China.

Author contribution statement

Q. J. H. proposed the hypotheses, conceived, designed and supervised the project, analyzed and interpreted the data, and wrote the paper. P.H.Z. initiated the research line under the assistance of Z. K. J. Z.K.J. performed chemical and biological experiments under the assistance of W. J. G. under the supervision of Q. J. H. and W. J. D.

Electronic Supplementary Material: Supplementary material (UV absorption spectra) is available in the online version of this article at https://doi.org/10.1007/s12274-022-4860-y.

References

[1] Dole, M.; Wilson, F. R.; Fife, W. P. Hyperbaric hydrogen therapy: A possible treatment for cancer. *Science* **1975**, *190*, 152–154.

[2] Ohsawa, I.; Ishikawa, M.; Takahashi, K.; Watanabe, M.; Nishimaki, K.; Yamagata, K. I.; Katsura, K.; Katayama, Y.; Asoh, S.; Ohta, S. Hydrogen acts as a therapeutic antioxidant by selectively reducing cytotoxic oxygen radicals. *Nat. Med.* **2007**, *13*, 688–694.

[3] Zheng, X. F.; Mao, Y. F.; Cai, J. M.; Li, Y. H.; Liu, W. W.; Sun, P. L.; Zhang, J. H.; Sun, X. J.; Yuan, H. B. Hydrogen-rich saline protects against intestinal ischemia/reperfusion injury in rats. *Free Radic. Res.* **2009**, *43*, 478–484.

[4] Wan, W. L.; Tian, B.; Lin, Y. J.; Korupalli, C.; Lu, M. Y.; Cui, Q. H.; Wan, D. H.; Chang, Y.; Sung, H. W. Photosynthesis-inspired H_2 generation using a chlorophyll-loaded liposomal nanoplatform to detect and scavenge excess ROS. *Nat. Commun.* **2020**, *11*, 534.

[5] Ichihara, M.; Sobue, S.; Ito, M.; Ito, M.; Hirayama, M.; Ohno, K. Beneficial biological effects and the underlying mechanisms of molecular hydrogen-comprehensive review of 321 original articles-. *Med. Gas. Res.* **2015**, *5*, 12.

[6] Zhou, G. X.; Goshi, E.; He, Q. J. Micro/nanomaterials-augmented

hydrogen therapy. *Adv. Healthcare Mater.* **2019**, *8*, 1900463.
[7] Gong, W. J.; Jiang, L. D.; Zhu, Y. X.; Jiang, M. N.; Chen, D. Y.; Jin, Z. K.; Qin, S. C.; Yu, Z. Q.; He, Q. J. An activity-based ratiometric fluorescent probe for *in vivo* real-time imaging of hydrogen molecules. *Angew. Chem., Int. Ed.* **2022**, *61*, e202114594.
[8] Yao, X. X.; Chen, D. Y.; Zhao, B.; Yang, B. R.; Jin, Z. K.; Fan, M. J.; Tao, G. R.; Qin, S. C.; Yang, W. L.; He, Q. J. Acid-degradable hydrogen-generating metal-organic framework for overcoming cancer resistance/metastasis and off-target side effects. *Adv. Sci. (Weinh.)* **2022**, *9*, 2101965.
[9] Zhao, B.; Wang, Y. S.; Yao, X. X.; Chen, D. Y.; Fan, M. J.; Jin, Z. K.; He, Q. J. Photocatalysis-mediated drug-free sustainable cancer therapy using nanocatalyst. *Nat. Commun.* **2021**, *12*, 1345.
[10] Zhao, P. H.; Jin, Z. K.; Chen, Q.; Yang, T.; Chen, D. Y.; Meng, J.; Lu, X. F.; Gu, Z.; He, Q. J. Local generation of hydrogen for enhanced photothermal therapy. *Nat. Commun.* **2018**, *9*, 4241.
[11] Lubitz, W.; Ogata, H.; Rüdiger, O.; Reijerse, E. Hydrogenases. *Chem. Rev.* **2014**, *114*, 4081–4148.
[12] Motterlini, R.; Otterbein, L. E. The therapeutic potential of carbon monoxide. *Nat. Rev. Drug Discov.* **2010**, *9*, 728–743.
[13] Szabo, C. Gasotransmitters in cancer: From pathophysiology to experimental therapy. *Nat. Rev. Drug Discov.* **2016**, *15*, 185–203.
[14] Carbonero, F.; Benefiel, A. C.; Gaskins, H. R. Contributions of the microbial hydrogen economy to colonic homeostasis. *Nat. Rev. Gastroenterol. Hepatol.* **2012**, *9*, 504–518.
[15] Ostojic, S. M. H_2 alter mitochondrial bioenergetics via GHS-R1α activation? *Theranostics* **2017**, *7*, 1330–1332.
[16] Needles, A.; Heinmiller, A.; Sun, J.; Theodoropoulos, C.; Bates, D.; Hirson, D.; Yin, M.; Foster, F. S. Development and initial application of a fully integrated photoacoustic micro-ultrasound system. *IEEE Trans. Ultrason. Ferroelect. Freq. Control* **2013**, *60*, 888–897.
[17] Xia, J.; Danielli, A.; Liu, Y.; Wang, L. D.; Maslov, K.; Wang, L. V. Calibration-free quantification of absolute oxygen saturation based on the dynamics of photoacoustic signals. *Opt. Lett.* **2013**, *38*, 2800–2803.